Surface-Enhanced Resonance Raman Spectroscopic and Electrochemical Study of Cytochrome c Bound on Electrodes through Coordination with Pyridinyl-Terminated Self-Assembled Monolayers

By: D. H. Murgida, P. Hildebrandt, J. Wei, Y.-F. He, Haiying Liu and D. H. Waldeck

D. Murgida, J. Wei, P. Hildebrandt, Y. F. He, H. Y. Liu, and D. H. Waldeck, "SERR and Electrochemical Study of Cytochrome c Bound on Electrodes through Coordination with Pyridinyl-terminated SAMs" *Journal of Physical Chemistry B*, **2004**,108, 2261-2269.

Abstract:

Cytochrome *c* (Cyt-*c*) is immobilized on Ag and Au electrodes coated with self-assembled monolayers (SAM), comprised of pyridine-terminated alkanethiols and a shorter chain diluent thiol. Surface-enhanced resonance Raman (SERR) spectroscopy of coated Ag electrodes reveals that the adsorbed Cyt-*c* forms a potential-dependent coordination equilibrium with a predominant five-coordinated high-spin (5cHS) state in the reduced form and six-coordinated low-spin (6cLS) state prevailing in the oxidized form. In the oxidized species, the native Met-80 ligand of the heme is replaced by a pyridinyl residue of the bifunctional thiols that according to earlier scanning tunneling microscopy form islands in the hydrophobic monolayer. The redox potentials derived from the SERR band intensities are estimated to be −0.24 and −0.18 V (vs AgCl) for the 6cLS and 5cHS states, respectively, and lie in the range of the midpoint potential determined for Cyt-*c* on coated Au electrodes by cyclic voltammetry (CV). Whereas in the latter case, a nearly ideal Nernstian behavior for a one-electron couple was observed, the SERR spectroscopic analysis yields about 0.4 for the number of transferred electrons for each spin state. This discrepancy is mainly attributed to a distribution of substates of the immobilized protein in both the 6cLS and 5cHS forms, as indicated by substantial band broadening in the SERR spectra. These substates may arise from different orientations and heme pocket structures and exhibit different redox properties. Whereas SERR spectroscopy probes all adsorbed Cyt-*c* species including those that are largely redox inactive, CV measurements reflect only the substates that are electrochemically active.

Keywords: redox chemistry | protein | Surface-enhanced resonance Raman (SERR) | Cytochrome c (Cyt-c)

Article:

Introduction

In the past few years, redox proteins adsorbed on electrodes have gained increasing attention both in physicochemical and biophysical studies.[1,2] In a practical sense, immobilized proteins represent key elements for bioelectronic devices with potential applications in biotechnology and nanotechnology. To fully exploit the functional properties of proteins and enzymes and to allow for rational design of tailor-made devices, detailed knowledge of the mechanism and dynamics of the interfacial processes, specifically heterogeneous electron transfer (ET) reactions, is required. In a fundamental sense, deeper insight into the underlying redox chemistry may contribute to a better understanding of the molecular processes of membrane-bound and membrane-associated proteins under physiological conditions.

In this respect, cytochrome *c* (Cyt-*c*) represents an ideal model protein inasmuch as its three-dimensional structure is well characterized,[3] and a large body of experimental data has been accumulated on its homogeneous and heterogeneous electron transfer reactions.[4-11] This heme protein offers the particular advantage that it can be immobilized on electrodes in a well-defined manner using quite different strategies. Because of its high molecular dipole moment and the clustering of cationic lysine residues on the front surface of the protein, Cyt-*c* binds electrostatically to anionic electrode surfaces in a largely uniform orientation. Such surfaces can be provided either by chemisorption of anions on electrode surfaces[11,12] or, more elegantly, by depositing self-assembled monolayers (SAM) of bifunctional thiols that carry negatively charged headgroups (carboxylate[7,8] or phosphate[13]). Alternatively, covalent attachment can be achieved by chemical cross-linking to the lysine residues on the front surface of the protein; however, the resultant orientational distribution of the bound proteins appears to be more heterogeneous than in the case of electrostatic binding.[8b] Also, immobilization via hydrophobic interactions has been shown on electrodes covered with SAMs of alkanethiols.[10] In this case, the protein is bound via a (partial) insertion of the hydrophobic amino acid segment 80−85 into the monolayer. Finally, it is also possible to attach the protein via direct coordination to the heme, by using SAMs of thiols that carry a headgroup such as pyridinyl that can effectively compete with the native Met-80 ligand for the axial coordination site of the heme.[9]

In these systems, the immobilized Cyt-*c* displays quite different redox properties with substantial variations in the redox potentials and the electron transfer kinetics.[9] For a comprehensive understanding of these processes, however, it is necessary to analyze how the variations in the thermodynamic and kinetic properties are related to the molecular structure of the immobilized protein. Surface-enhanced resonance Raman (SERR) spectroscopy can provide such information because this technique selectively probes the redox sites, that is, the heme groups of the immobilized proteins, and allows monitoring of potential-dependent changes in the molecular structure.[14] By combining this technique with the potential-jump method, it is possible to study the electron transfer dynamics of the immobilized species and gain valuable insight into the molecular mechanism of the interfacial redox process. Previous studies applied this approach to electrostatically,[8] hydrophobically,[10] and covalently bound Cyt-*c*;[8b] the present work is dedicated to the analysis of the redox process of Cyt-*c* directly linked to an electrode via axial coordination of a pyridinyl residue. In addition to electrochemical techniques and scanning tunneling microscopy (STM), which have been used in previous studies,[9] we have employed SERR

spectroscopy for a comprehensive analysis of the thermodynamic and structural aspects of the redox behavior of the bound Cyt-*c*.

Materials and Methods

Chemicals. Bis[11-((4-pyridinylcarbonyl)oxy)undecyl]disulfide (C11py) and bis[12-((pyridinylcarbonyl)oxy)dodecyl]disulfide (C12py) were prepared in the manner described previously.[9c,d] Horse heart cytochrome *c* (Sigma, type VI) was chromatographically purified according to previously published procedures.[9c,d,15] The 11-mercapto-1-undecanol (97%), 1-octanethiol (>98.5%), 1-hexadecanethiol, and 1-undecanethiol (>98%) were purchased from Aldrich and used without further purification. Absolute ethanol was purchased from Pharmco Products, Inc.; water for experiments was purified by using a Barnstead-Nanopure system and had a resistivity of 18 MΩ-cm.

SERR Electrode Preparation. Silver electrodes were electrochemically roughened as described before[16] and then immersed in ethanolic solutions of 1:9 mixtures of a pyridinyl-terminated alkanethiol and a diluent alkanethiol (1 mM total) for a period of 1−3 days to create mixed self-assembled monolayers (SAM). For 1:9 mixtures of 4-pyridinyl-CO_2-$(CH_2)_{11}$-SH/1-octanethiol or 4-pyridinyl-CO_2-$(CH_2)_{11}$-SH/1-decanethiol the SAMs are denoted as Py-H, whereas SAMs obtained with 1:9 mixtures of 4-pyridinyl-CO_2-$(CH_2)_{12}$-SH/11-mercapto-1-undecanol are denoted as Py-OH. After the electrodes were rinsed with ethanol and dried under an Ar stream, they were immersed in the electrochemical cell containing roughly 0.5 μM Cyt-*c* in a 20 mM phosphate buffer at pH 7.0. The protein was allowed to adsorb for 60 min at open circuit and under purging with Ar.

Gold Electrode Preparation. For cyclic voltammetry (CV) studies, the gold (99.99% Aldrich) electrodes were prepared in the same procedure as before[9c] with a tip of exposed area of 0.06−0.12 cm^2. For the STM studies, a Au(111) facet of a single crystalline bead (prepared by Clavilier's method[17]) was used as the substrate and cleaned thoroughly before SAM preparation. The SAM preparation on gold electrodes, for both the cyclic voltammetry and the STM measurements, proceeded in the same way as that on the silver electrodes. The electrodes were rinsed with ethanol and dried under an Ar gas stream.

Cyclic Voltammetry. Cyclic voltammetry on the immobilized Cyt-*c* was carried out with an EG&G PAR-283 potentiostat, which was controlled by a Pentium computer running version 4.3 of PARC Model 270 software and a GPIB board. The three-electrode cell had a platinum spiral counter electrode, a Ag/AgCl (3 M NaCl) reference electrode, and the surface-modified working electrode. The voltammetry measurements were performed in 20 mM phosphate buffer solution (pH of 7.0) under an argon atmosphere. After measurement, the SAM on the gold bead was removed by immersing it in a "piranha" solution (a mixture of 30% H_2O_2 and 98% H_2SO_4 in a 1:3 volume ratio) for 20 s. The bead area was determined by running voltammetry in a 0.5 M KCl solution that contained 1 mM $K_3[Fe(CN)_6]$ and 1 mM $K_4[Fe(CN)_6]$. [9c,18]

The capacitance of the SAM was estimated from the charging current of the voltammograms during the cyclic voltammetry measurement.

$$\frac{dQ}{dt} = C\frac{dV}{dt} \quad \text{that is,} \quad i = Cv$$

where Q is the charge, C is the capacitance, V is the potential of a parallel plate capacitor, i is the charging current, and v is the voltage scan rate. The voltammograms give average capacitances of 1.2 μF/cm^2 for a 1-day electrode and 1.22 μF/cm^2 for a 3-day electrode, corresponding to a film thickness 16.8 Å and 16.5 Å, respectively.[19] Of course, such a simple model does not adequately describe electrochemical interfaces.[20] However, given this caveat it is apparent that the film thickness is very close to that expected from simple bond length calculations.

SERR Measurements. SERR spectra were measured with the 413-nm excitation line of a Kr^+-laser (Coherent Innova 302) using a spectrograph (U1000, ISA) equipped with a liquid nitrogen cooled charge-coupled device (CCD) camera. The spectral resolution was 4 cm^{-1} and the step width (increment per data point) was 0.53 cm^{-1}. Accumulation times of the spectra were 10−40 s. The laser beam (ca. 60 mW) was focused onto the surface of a rotating Ag electrode in a home-built thermostated electrochemical cell, which permits temperature control within ±0.1 °C. The SAM-modified Ag electrode was in contact with a solution containing the supporting electrolyte (20 mM potassium phosphate buffer at pH = 7) and roughly 0.5 μM Cyt-*c*. All potentials refer to the Ag/AgCl electrode. Measurements were performed under continuous purging with argon. Stationary spectra were measured at several potentials between +0.1 V and −0.6 V.

STM Measurements. The STM images were obtained with a Nano IIIA STM system (Digital Instruments). STM tips were cut by using 0.25 mm diameter Pt−Ir wires (Goodfellow). All the STM images were obtained in air under constant current mode at 50−100 pA and a tip−sample bias of 0.8−1.0 V. Two different sample preparations of the ω-hydroxyalkanethiol mixture (C12py/C11OH) are presented. They differ by the exposure time, 1 day versus 3 days, of the electrode to the solution mixture of alkanethiols. The measurements were reproduced twice.

Results

Cyt-*c* was adsorbed on Ag electrodes that were coated with SAMs of Py-H. By using SERR spectroscopy, the redox equilibria and the heme pocket structure of the adsorbed protein were probed as a function of the electrode potential. The spectra were measured in the high-frequency region between circa 1300 and 1700 cm^{-1} to probe the ν_3 and ν_4 vibrational modes. These modes provide sensitive markers for the coordination, spin, and redox state of the heme iron.[12] Visual inspection of the spectra measured at two extreme potentials, 0.1 V and −0.5 V, at which the sample is expected to be nearly fully oxidized and fully reduced respectively, indicates the coexistence of two different Cyt-*c* species at each potential (Figure 1). At 0.1 V, the ν_3 region displays a peak at 1504 cm^{-1}, which is typical for a six-coordinate low-spin oxidized ($6cLS^{Ox}$) heme, and a shoulder at circa 1491 cm^{-1} characteristic of a five-coordinate high-spin oxidized ($5cHS^{Ox}$) heme. In addition, the ν_4 band is centered at circa 1373 cm^{-1}, which is also indicative of a $6cLS^{Ox}$ heme. A simple band-fitting analysis shows that, on the low-frequency side, this peak deviates from a single Lorentzian band shape, indicating the superposition by at least one further band at slightly lower frequencies expected for a $5cHS^{Ox}$ heme. At −0.5 V the situation is reversed, such that the ν_4 band is found at circa 1354 cm^{-1}, a position typical for $5cHS^{Red}$ hemes, and the deviation from the Lorentzian shape is now observed on the high-frequency side, that is, in the region expected for a $6cLS^{Red}$ form. Additionally, the ν_3 region exhibits two weaker bands

at 1467 and 1491 cm^{-1} that are clear indications for $5cHS^{Red}$ and $6cLS^{Red}$ Cyt-*c*, respectively. Also evident in Figure 1 are bands centered around 1590 cm^{-1}; however, these are not very reliable markers and are not discussed. Thus, the potential-dependence of the shape and position of the ν_3 and ν_4 bands suggest a conformational equilibrium of the adsorbed protein that is dominated by a 6cLS and a 5cHS form in the oxidized and reduced state, respectively.

SERR spectra measured as a function of the electrode potential between −0.6 and 0.1 V in 50 mV steps (data not shown) display a gradual transition between the two extreme cases represented in Figure 1. A sound quantitative analysis of the coupled redox and conformational equilibria requires knowledge of the component spectra for the four species that are involved, that is, $6cLS^{Red}$, $6cLS^{Ox}$, $5cHS^{Red}$, and $5cHS^{Ox}$. Because these species cannot be prepared in a pure form, their component spectra are not known a priori. Rather, they must be determined iteratively, in a manner described previously.[21] The resonance Raman (RR) and SERR spectra of native and non-native 6cLS and 5cHS species of Cyt-*c*, which were analyzed in detail previously,[12] were chosen as an initial set of spectra. The spectral parameters (positions, bandwidths, and relative intensities) for each redox and coordination state ($6cLS^{Red}$, $6cLS^{Ox}$, $5cHS^{Red}$, and $5cHS^{Ox}$) were varied iteratively to obtain a consistent fit to all the experimental data by using only the relative contributions of the individual species as adjustable parameters (Figure 2, Table 1). Figure 3shows the relative contributions of the different species to the spectra, as a function of electrode potential. At very negative potentials the spectra are dominated by the $5cHS^{Red}$ component, but at positive values the $6cLS^{Ox}$ form becomes the most intense one, confirming the idea of a redox state dependent coordination equilibrium for the adsorbed protein.

The relative spectral contributions are proportional to the relative concentrations of the different species; however, the respective proportionality factors, which are unknown, are likely to be different. Therefore, the data in Figure 3 represent only semiquantitative potential-dependencies of the populations of the various Cyt-*c* species. Nevertheless, it can be concluded that the adsorbed Cyt-*c* forms a potential-dependent conformational equilibrium that is dominated by a $5cHS^{Red}$species at negative values and a $6cLS^{Ox}$ one at positive potentials.

In another series of experiments, the alkyl-terminated diluent thiols in the mixed monolayer films were replaced by hydroxyl-terminated thiols. Earlier work has shown that Cyt-*c* does not directly adsorb to hydroxyl-terminated layers,[8c,22] whereas it does adsorb to alkyl-terminated layers.[10]The Py-OH monolayers were characterized by cyclic voltammetry, STM, and SERR spectroscopy. These measurements indicate a very poor adsorption of Cyt-*c* to the surface. From the SERR measurements on Ag/Py-OH (Figure 4) the coverage is estimated to be about 2% of that obtained on Py-H monolayers. The low signal-to-noise ratio of the SERR spectra under these conditions impedes any further analysis.

Cyclic voltammetry and STM measurements were performed for two different preparations of the hydroxyl-terminated electrodes. The two preparations differed by the exposure time of the electrode to the deposition solution (1 part pyridine-terminated alkanethiol and 9 parts hydroxyl-terminated thiol), for 1 day (1-day electrode) and 3 days (3-day electrode). The two voltammograms in Figure 5 were obtained after these electrodes had been incubated in a Cyt-*c*solution for 40 min, then washed and studied in a buffer solution. The flatter curve was obtained from the 3-day electrode and the other curve, with a pronounced faradaic current, resulted from

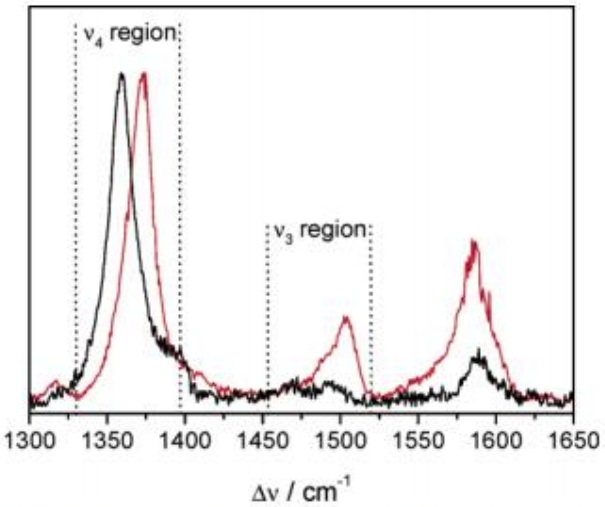

Figure 1. SERR spectra of Cyt-*c* adsorbed to a Py-H-coated Ag electrode at −0.5 V (black) and 0.1 V (red).

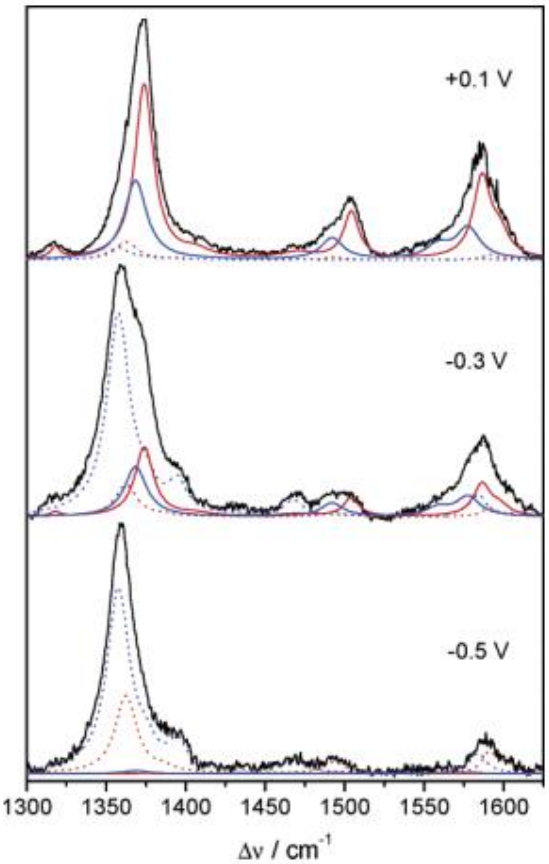

Figure 2. Experimental SERR spectra of Cyt-*c* adsorbed on Py-H-coated electrodes at different potentials. The component spectra of the various species are given by different line shapes and colors: blue solid, $5cHS^{Ox}$; blue dotted, $5cHS^{Red}$; red solid, $6cLS^{Ox}$; red dotted, $6cLS^{Red}$ (cf. Table 1).

TABLE 1: Frequencies and Band Widths (in Parentheses) of the SERR Marker Bands ν_3 and ν_4 of the Various Cyt-*c* Species

species	ν_3 (cm^{-1})	ν_4 (cm^{-1})
$6cLS^{Red}$ (Py-H)[a]	1493.6(14.4)	1362.5(16.4)
$6cLS^{Ox}$ (Py-H)[a]	1504.2(11.7)	1373.9(14.1)
$5cHS^{Red}$ (Py-H)[a]	1467.8(14.4)	1357.6(17.4)
$5cHS^{Ox}$ (Py-H)[a]	1492.0(16.6)	1368.5(16.9)
$6cLS^{Red}$ (B1)[b]	1490.7(13.1)	1360.2(9.5)
$6cLS^{Ox}$ (B1)[b]	1501.1(11.9)	1371.0(15.2)
$6cLS^{Red}$ (B2)[c]	1492.5(13.5)	1359.0(12.0)
$6cLS^{Ox}$ (B2)[c]	1503.0(12.3)	1373.0(15.9)
$5cHS^{Red}$ (B2)[c]	1471.0(15.0)	1353.0(12.5)
$5cHS^{Ox}$ (B2)[c]	1489.0(14.5)	1369.0(12.7)

[a] Cyt-*c* species on Py-H-coated electrodes (this work). [b] B1 refers to the native protein.[12] [c] B2 denotes the non-native conformational states obtained upon electrostatic or hydrophobic interactions.[12]

the 1-day electrode. The lack of significant faradaic current from the 3-day electrode illustrates that little or no Cyt-*c* is adsorbed on the electrode, whereas the 1-day electrode shows a weak faradaic response. The full width at half-maximum of the reduction peak for the 1-day electrode is 88 mV. Analysis of the reduction peak gives a Cyt-*c* coverage of 0.21 pmol/cm^2, from both the peak current and the peak charge integral.[23] This coverage is 8−9% of that for the Py-H system reported previously.[9c]

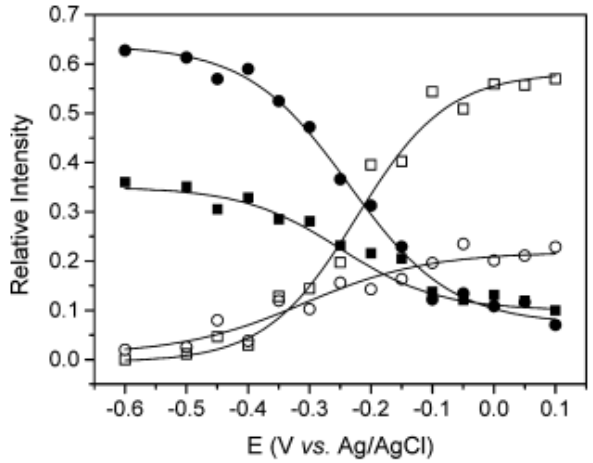

Figure 3. Potential-dependent distribution of species of Cyt-*c* adsorbed on Py-H-coated electrodes expressed in relative intensities: solid squares, 6cLS^{Red}; hollow squares, 6cLS^{Ox}; solid circles, 5cHS^{Red}; hollow circles, 5cHS^{Ox}.

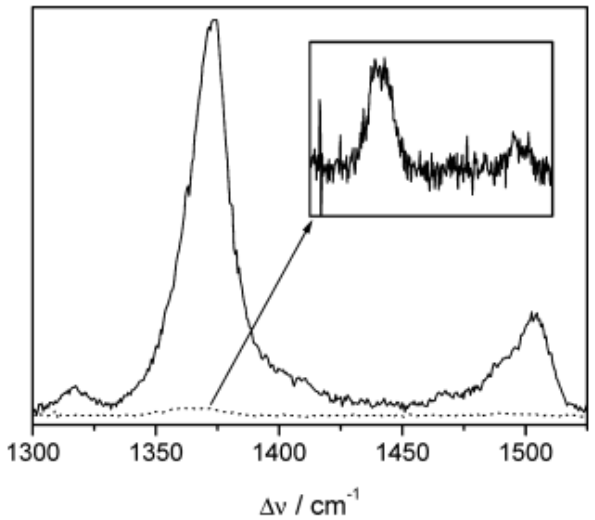

Figure 4. SERR spectra of Cyt-*c* adsorbed on Py-H (solid line) and Py-OH (dotted line and inset) monolayers measured under identical conditions.

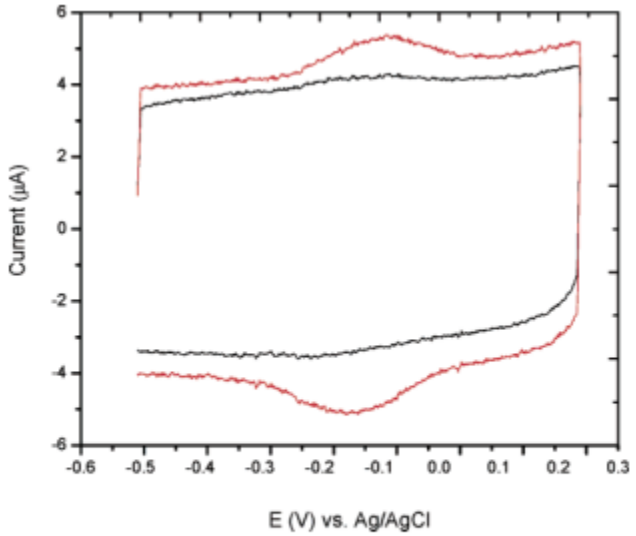

Figure 5. Cyclic voltammograms of Cyt-*c* immobilized on a gold electrode coated with a Py-OH self-assembled monolayer. The two curves are the response from the electrode incubated in Py-OH ethanol solution for 3 days (black) and 1 day (red) at a scan rate of 30 V/sec in a buffer solution at pH 7.

STM images of these two electrode preparations are shown in Figure 6. Panel A shows images for the 3-day preparation, and panel B shows images for the 1-day preparation. The primary difference to note between these two images is the presence of bright spots (elevated regions) on the images for the 1-day electrode preparation (panel B). The cross-section shown below Figure 6B intersects three of the elevated spots in the image, for which the heights range from 3 to 5 Å. The height difference is in reasonable agreement with the 6 Å expected for these hydroxy-terminated and pyridine-terminated thiols from simple bond length estimates.[24] These elevated regions are similar to those observed previously for Py-H/alkanethiol mixed systems.[9c] An analysis of this image indicates that the elevated regions occupy 1.5% to 2% of the total area.[25]

In contrast to the 1-day electrode, the images of the 3-day electrode (Figure 6A) do not display elevated regions. This result suggests that prolonged exposure of the electrode to the thiol solution leads to the formation of a nearly pure hydroxyl-terminated thiol monolayer, to the exclusion of the pyridine-terminated thiol. This finding is substantiated by the failure to observe faradaic current or a SERR signal on the 3-day electrodes.

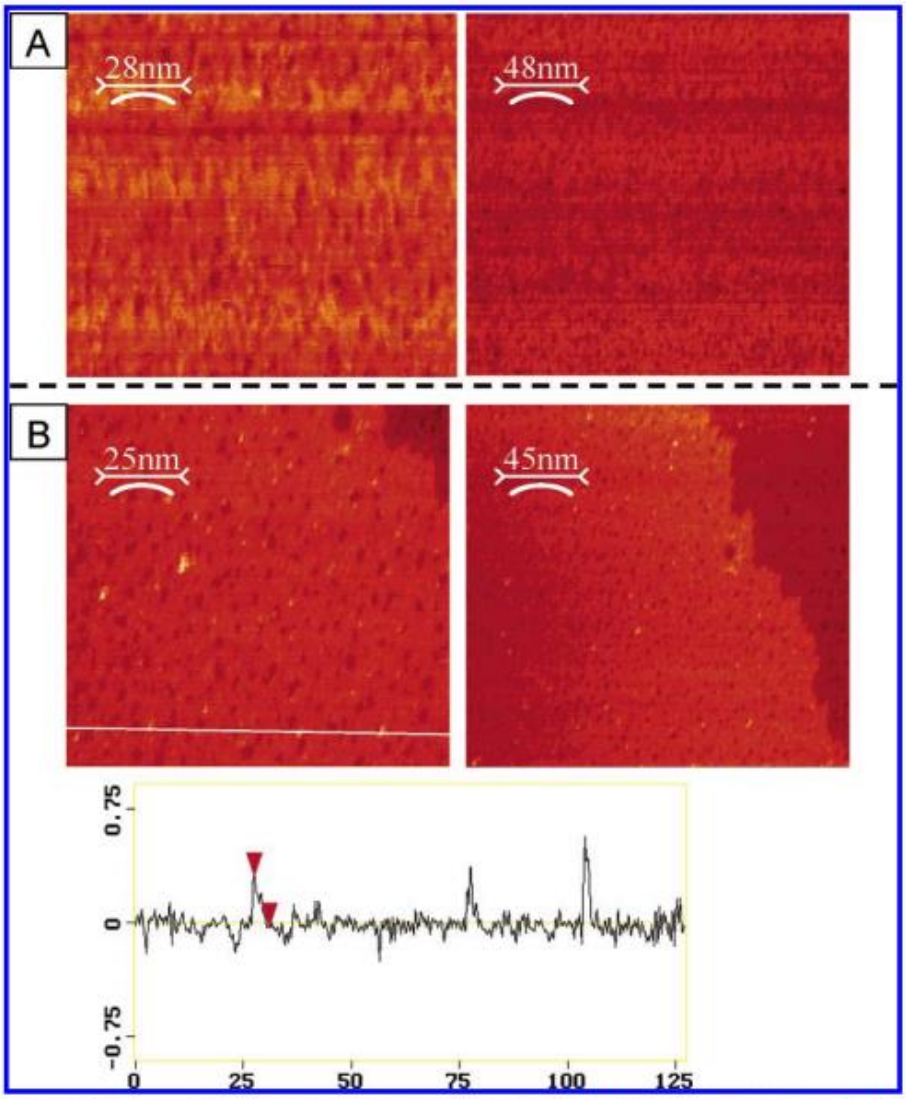

Figure 6. STM images of a gold electrode incubated in an ethanolic Py-OH solution (1:9 molar ratio of C12py and C11OH) for 3 days (A) and 1 day (B).

Discussion

Conformational Equilibria. The potential-dependent SERR measurements of Cyt-*c* adsorbed on Py-H-coated Ag electrodes clearly indicates a redox-coupled conformational equilibrium between two forms of the adsorbed protein that are assigned to 6cLS heme and 5cHS heme configurations (Figure 3). Figure 7 shows a square reaction scheme that can account for these observations.

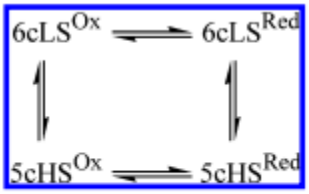

Figure 7. Redox and conformational equilibria of Cyt-*c* adsorbed to Py-H-coated electrodes.

Previous SERR and RR studies in our group have shown that when Cyt-*c* is electrostatically adsorbed to negatively charged model systems, for example, Ag electrodes coated with ω-carboxyl alkanethiols, the native protein (B1) is in equilibrium with a new conformational state B2.[8c,11,12] The formation of the B2 state is induced by the local electrostatic field at the binding domain. This field arises from the array of negative charges on the SAM surface interacting with the positively charged lysine groups on the surface of Cyt-*c* and by the external field caused by the polarization of the metal electrode and the potential drop across the SAM. The main structural difference between the B2 conformational state and the native protein is the lack of the ligand Met-80 at the sixth axial position of the heme Fe. The axial position can either remain vacant, yielding a 5cHS heme, or be occupied by His-33 to form a new 6cLS configuration.

Recently, we reported the immobilization of Cyt-*c* on Ag electrodes coated with hydrophobic SAMs.[10] In this case, binding occurs via the hydrophobic patch, which includes the surface residues I85, G84, A83, F82, and I81. This patch is located in the center of the ring of lysine residues, in close vicinity to the partially exposed heme edge (Figure 8A). In this case, the driving force for adsorption is the entropy gained by minimizing the solvent-exposed hydrophobic area. The interactions between the hydrophobic peptide segment and the SAM are hypothesized to induce the rupture of the Fe−Met-80 bond, which leads to a 5cHS heme and subsequently to a new 6cLS form, in which His-33 is likely the sixth ligand. Although the mechanisms are totally different, both electrostatic and hydrophobic interactions between the SAM and the front face of Cyt-*c* induce conformational equilibria that, with respect to the spin and coordination state of the heme, are similar to those found for Cyt-*c* bound to Py-H monolayers. In this sense, the adsorption properties of the different systems are similar.

Characterization of the Py-H mixed monolayers on Au by STM and cyclic voltammetry[9c] showed that the pyridinyl headgroups constitute 1−4% of the modified Au surface. Thus, a priori, one cannot discard the possibility that Cyt-*c* binds to Py-H-coated electrodes via the hydrophobic region of the SAM, that is, without the involvement of the pyridinyl headgroups. However, several observations indicate that adsorption through hydrophobic binding may hold, if at all, only for a very small fraction of the adsorbed Cyt-*c* molecules. In earlier work, the Au bead electrodes coated with only alkanethiol did not reveal

any obvious Faradaic current, whereas the mixed films display a strong Faradaic signal. In addition, the apparent redox potential was shifted about 170 mV negative of that for the native form. This redox potential corresponds well to that found in solution for pyridine coordinated to Cyt-*c*'s heme with a largely preserved protein secondary structure.[26]

The most compelling evidence for ligation of Cyt-*c* with the pyridine headgroup, rather than the alkanethiol diluent, comes from the SERR spectra. The SERR spectra show that the conformational equilibrium on the Py-H films is shifted significantly from that on pure alkanethiol films. For Cyt-*c* adsorbed on purely hydrophobic alkanethiol monolayers, the conformational equilibrium of the oxidized protein is completely shifted toward the B2 forms (6cLS and 5cHS), whereas in the reduced state only the native 6cLS form (B1) is detected. In contrast, on Py-H monolayers ferrous Cyt-*c* mainly exists in the 5cHS form. In addition, the component spectra that are determined for the different redox and ligation states of Cyt-*c* immobilized on Py-H monolayers differ from the so-called B1 and B2 forms. Specifically, the bands ν_3 and ν_4 of the 6cLS form are shifted to higher wavenumbers with respect to the corresponding modes of the B1 and B2 states and also show some differences in relative intensities both in the reduced and oxidized state (Figure 9, Table 1). In addition, the 6cLS component exhibits significant spectral differences with respect to the alkaline forms of the protein.[27] These differences suggest that the sixth ligand cannot be assigned to Met-80 (B1), His-33 (B2), or a lysine residue (alkaline form). Instead, the 6cLS species in both redox states most likely corresponds to the pyridinyl-coordinated heme. Also the 5cHS form exhibits spectral differences with respect to the B2 5cHS species on pure hydrophobic monolayers, especially for the ν_3 band (Table 1). This comparison further indicates that at least the major fraction of the 5cHS species does not result from proteins immobilized on the hydrophobic regions of the Py-H SAMs.

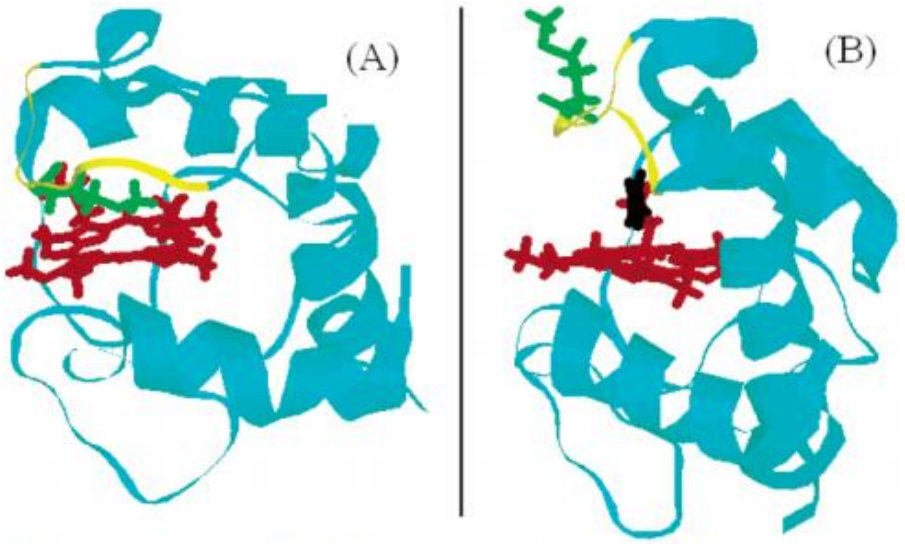

Figure 8. Solution structures of ferric Cyt-*c* (A, PDB-1AKK) and the complex with imidazole (B, PDB-1F17): red, heme; green, Met-80; yellow, peptide segment 77−85; black, imidazole.[30]

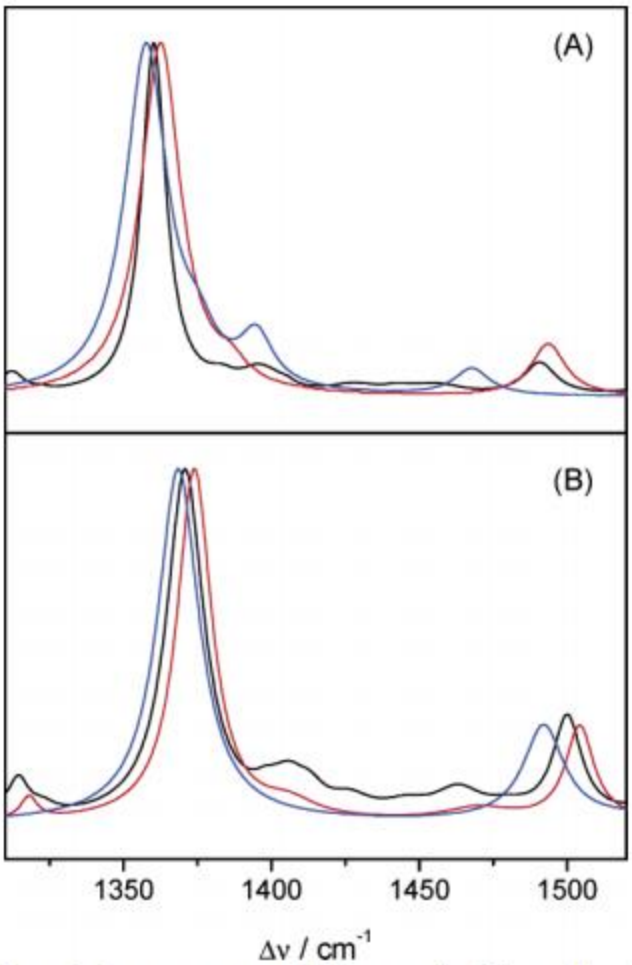

Figure 9. Component spectra of different species of ferrous (A) and ferric (B) Cyt-*c*: black, native protein (B1); red, 6cLS form on Py-H monolayers; blue, 5cHS form on Py-H monolayers.

The specific interactions of the protein with the Py-H monolayers and the differences with respect to purely hydrophobic or electrostatic adsorption are reflected in the width of the band ν_4, which is an indicator of the flexibility or stability of the heme pocket. In native Cyt-*c*, the ν_4 bandwidth of the ferric form is broader by 60% than that of the more stable ferrous form. Also, in the non-native 6cLS conformations that are induced by purely hydrophobic or electrostatic interactions of the protein with appropriate model systems, the ν_4 band envelopes of the oxidized forms are always broader by at least 20% than those of the reduced forms. In contrast, for Cyt-*c* adsorbed to Py-H monolayers the ν_4 band of the 6cLS form is narrower by 20% in the oxidized state than in the reduced state, indicating that the heme pocket stability is reversed. This observation can be attributed to the higher stability of the pyridine−Cyt-*c* complex in the ferric state compared to the ferrous state. On the other hand, in the 5cHS conformation, the bandwidth of ν_4 does not change significantly with the oxidation state, as expected.

Upon substitution of Met-80 by an external ligand, the entire loop 77−85 is shifted away from the heme such that Met-80 points away from the protein interior, as shown in Figure 8B for the NMR structure of the imidazole complex of Cyt-*c* in solution. Thus, the hydrophobic segment 80−85 becomes more flexible and solvent exposed. In the 6cLS form of Cyt-*c* bound to Py-H

SAM the pyridinyl group serves as the external ligand, and it is likely that the displaced peptide segment 80−85 interacts with the hydrophobic chains of the monolayer, stabilizing the complex. This interpretation is consistent with the drastically weaker adsorption of Cyt-*c* on SAMs of mixed pyridinyl/hydroxyl-terminated thiols (Figure 4), even though the pyridinyl coverage on the film is similar (within a factor of 2). The hydrophobic interactions should persist when the coordinative pyridinyl−iron bond is broken in the 5cHS form. Furthermore, it is likely that the pyridinyl group remains in the heme pocket and prevents the Met-80 from rebinding to the ferrous heme, in contrast to the case of Cyt-*c* immobilized on purely hydrophobic monolayers. This scenario explains why the native B1 form is recovered for the reduced state at hydrophobic electrodes but not for the Py-H-coated electrodes. In addition, these conclusions are in agreement with the apparent increase in the 6cLS/5cHS equilibrium constant by a factor of about 5 (Figure 3) from the reduced (−0.6 V) to the oxidized (0.1 V) couple, which is consistent with the larger affinity of exogenous N-ligands for the ferric form of Cyt-*c*.

A related scenario has been observed for the formation of the bis-His complex of Cyt-*c* upon sodium dodecyl sulfate (SDS) binding in solution. At submicellar concentrations, SDS molecules interact with the hydrophobic patch of the protein and destabilize the heme pocket, such that complete complexation with His-33 is achieved for ferric cytochrome *c*, whereas in the reduced protein the 5cHS state is stabilized under the same conditions.[12]

Redox Equilibria. The redox equilibria for both individual redox couples in Figure 7 can be analyzed according to the Nernst equation

$$E = E^0 - \frac{RT}{nF} \ln\left(\frac{I_{\mathrm{Red}} f_{\mathrm{Red}}}{I_{\mathrm{Ox}} f_{\mathrm{Ox}}}\right)$$

where I_i and f_i represent the absolute intensities and the inverse relative SERR cross-sections, respectively. Because the f_i factors are unknown, the determination of the apparent redox potentials was based only on the relative SERR intensities, that is, assuming $f_{\mathrm{Red}} = f_{\mathrm{Ox}}$. The Nernst plots show clear deviations from linearity, especially at high potentials, and an apparently linear region around the zero point of the ordinates, that is, in the vicinity of the apparent redox potential, as shown in Figure 10 for the 6cLS redox couple. Restricting the analysis to this linear region, apparent redox potentials of −0.24 V and −0.18 V are obtained for the 6cLS and 5cHS forms, respectively. The values for *n* were found to be only about 0.4 in each case. Both redox potentials are more positive than those found for the state B2 induced upon electrostatic adsorption (ca. −0.38 and −0.43 V).[11] Such positive shifts may reflect interactions between the hydrophobic chains in the Py-H monolayer and the peptide segment 80−85, which is likely to restrict solvent accessibility to the heme. Taking into account the uncertainty associated with the assumption $f_{\mathrm{Red}} = f_{\mathrm{Ox}}$, the apparent redox potential for the 6cLS couple determined by SERR spectroscopy is similar to that of the midpoint potential derived from CV, and both values exhibit comparable negative shifts with respect to the redox potential of the native protein in solution. Note that for both methods the values are more consistent with that found in solution for pyridine ligated to the heme iron with the protein in a largely preserved secondary structure (ca. −0.17 V)[26]than with the denatured pyridine/cytochrome *c* complex (ca. −0.33 V).[26]

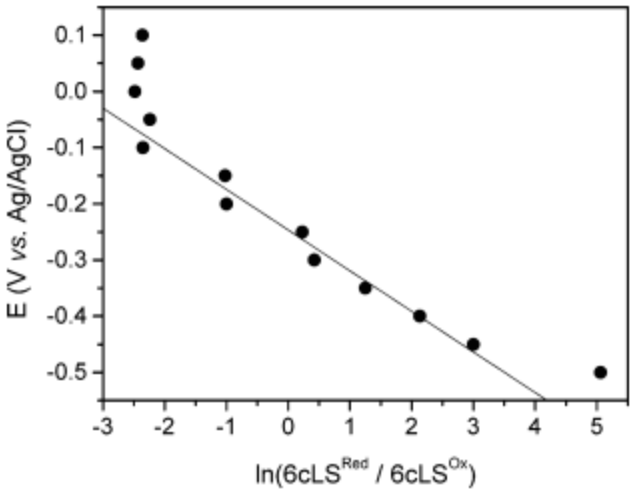

Figure 10. Nernstian plot for the 6cLS couple of Cyt-*c* adsorbed on Py-H monolayers. Further details are given in the text.

The square reaction scheme in Figure 7 provides a first approximation that accounts for the four spectroscopically distinguishable species. The underlying assumptions in this model are that the four cytochrome *c* species are electroactive and have a well-defined and potential-independent orientation with respect to the electrode, such that the system can be described with only two redox potentials. The broadening of the SERR bands, which is especially evident for the reduced forms of 5cHS and 6cLS (see Table 1), suggests a distribution of substates. These substates are not distinguishable on the level of the present SERR spectra and may only differ with respect to the orientation of the protein relative to the SAM surface, which in turn affects the solvent accessibility of the heme and could lead to a distribution of redox potentials. In addition, a subset of orientations may be unfavorable for electron transfer, and those species do not participate in the redox process. As in the case of Cyt-*c* electrostatically adsorbed to carboxyl-terminated SAMs,[8a]the orientational distribution might be potential-dependent, which could explain the deviations from an ideal Nernstian behavior at extreme electrode potentials. In fact, the experimental data in Figure 10 can be simulated by a Gaussian distribution of redox potentials centered at circa −0.24 V plus a fraction of redox inactive 6cLS ferrous Cyt-*c*.

Thus, for Cyt-*c* adsorbed to Py-H-coated Ag electrodes, stationary SERR measurements clearly show the existence of two redox couples (6cLS and 5cHS) with a nonideal electrochemical response. On the other hand, cyclic voltammetry experiments performed on the same system but using Au electrodes show only one redox couple ascribed to the Py-coordinated heme (6cLS) and a nearly ideal electrochemical response for scan rates faster than 1 V/s.[9b,c] In previous work, the standard heterogeneous electron transfer rate constant of Cyt-*c* on Py-H films was determined by measuring the peak potential separation as a function of the voltage scan rate.[9b,c] That analysis gave a rate constant of 780 ± 40 s^{-1}. The voltammogram in Figure 5 for Cyt-*c* adsorbed on the same tether but with a hydroxyl diluent, to eliminate partial unfolding from hydrophobic interactions and eliminate direct hydrophobically adsorbed protein, gives a rate constant of 760 s^{-1}. The correspondence in these rate constants suggests that the electron transfer rate is controlled by the coordination with the heme through the pyridinyl tether and that partial unfolding of the protein's hydrophobic region has little effect.

These apparent contradictions between the SERR and CV results can be rationalized in terms of structural differences of the SAMs on the two different metals and kinetic arguments based on the square reaction scheme in Figure 7. Previous studies have shown that alkanethiols form more densely packed SAMs on Ag than on Au, as is reflected, for example, in a higher resistance to ion transport.[28] Therefore, one should expect a smaller amount of 5cHS species on Py-H-coated Au electrodes compared to the more hydrophobic preparations on Ag. If in addition, the rate constants for the 6cLS to 5cHS conformational transitions and the heterogeneous electron transfer rate constant for the 5cHS species are much smaller than the scan rate, then the electrochemical response should be largely dominated by the 6cLS redox couple. For scan rates faster than 1 V/s, rate constants smaller than 0.7 s^{-1} can fulfill these conditions.

Time-resolved SERR measurements of Cyt-*c* adsorbed on Ag electrodes coated with ω-carboxyl alkanethiols show that the B1 to B2 transition is at least 3 orders of magnitude slower than the heterogeneous electron transfer of the B1 species.[29] On the other hand, in the electron-tunneling regime, the heterogeneous electron transfer rate constant of Cyt-*c* electrostatically adsorbed on carboxyl-terminated SAMs is roughly 200 times smaller than that of the directly linked heme on Py-H monolayers of comparable length.[9b] The reason for such a difference is the stronger electronic coupling in the second case. One could expect an even more dramatic difference between the 6cLS and 5cHS forms on Py-H SAMs because the orientation of the latter species is certainly not optimized for electron transfer.

Conclusions

1. The SERR spectra demonstrate that the redox center of cytochrome *c* can be directly linked to a silver electrode by coating the metal surface with mixed SAMs of Py-H, in which the pyridinyl headgroups are able to substitute for the natural axial ligand Met-80. The concomitant displacement of the peptide segment 80−85 from the heme pocket further stabilizes the complex via hydrophobic interactions with the alkyl-terminated thiols.

2. In line with the redox-dependent binding constant of the pyridinyl residue to the heme, this complex is more stable in the ferric than in the ferrous form leading to a redox-dependent spin and coordination equilibrium.

3. In both the 6cLS and the 5cHS states, the protein is most likely not adsorbed in a uniform orientation with respect to the plane of the electrode but rather exists in a distribution of orientations (substates) that correspond to a distribution of redox potentials. This distribution can account for the non-Nernstian behavior observed in the SERR spectroscopic analysis of Cyt-*c* on the coated Ag electrode.

4. The CV data reveal a nearly ideal Nernstian behavior for Cyt-*c* immobilized on a coated Au electrode. This discrepancy may be rationalized in terms of a fraction of the adsorbed proteins with very slow ET kinetics that does not contribute to the CV signals but is probed in the SERR experiments.

Acknowledgment

This work was supported by Fundação para a Ciência e a Tecnologia, Portugal (Grant POCTI/QUI/43323/2001), the Deutsche Forschungsgemeinschaft (Grant SFB498), and the U.S. National Science Foundation (Grant CHE-0111435).

References and Notes

(1) *Electroanalytical Methods for Biological Material*; Brajter-Toth, A., Chambers, J. Q., Eds.; Marcel Dekker: New York, 2002.

(2) Willner, I.; Katz, E. *Angew. Chem., Int. Ed.* **2000**, *39*, 1180−1218.

(3) (a) *Cytochrome c*−A Multidisciplinary Approach; Scott, R. A., Mauk, A. G., Eds.; University Science Books: Sausalito, California, 1995. (b) Moore, G. R.; Pettigrew, G. W. *Cytochromes c: Evolutionary, Structural andPhysicochemical Aspects*; Springer: New York, 1990.

(4) (a) Casimiro, D. R.; Richards, J. H.; Winkler, J. R.; Gray, H. B. *J. Phys. Chem.* **1993**, *97*, 13073−13077. (b) Luo, J.; Reddy, K. B.; Salameh, A. S.; Wishart, J. F.; Isied, S. S. *Inorg. Chem.***2000**, *39*, 2321−2329. (c) Mines, G. A.; Bjerrum, M. J.; Hill, M. G.; Casimiro, D. R.; Chang, I. J.; Winkler, J. R.; Gray, H. B. *J. Am. Chem. Soc.* **1996**, *118*, 1961−1965. (d) Winkler, J. R.; Di Bilio, A. J.; Farrow, N. A.; Richards, J. H.; Gray, H. B. *Pure Appl. Chem.* **1999**, *71*, 1753−1764.

(5) (a) Harris, M. R.; Davis, D. J.; Durham, B.; Millett, F. *BBABioenerg.* **1997**, *1319*, 147−154. (b) Mclendon, G. *Acc. Chem. Res.* **1988**, *21*, 160−167. (c) Mei, H. K.; Wang, K. F.; Peffer, N.; Weatherly, G.; Cohen, D. S.; Miller, M.; Pielak, G.; Durham, B.; Millett, F.*Biochemistry* **1999**, *38*, 6846−6854. (d) Pletneva, E. V.; Fulton, D. B.; Kohzuma, T.; Kostic, N. M. *J. Am. Chem. Soc.* **2000**, *122*, 1034−1046.

(6) (a) Armstrong, F. A.; Hill, H. A. O.; Walton, N. J. *Acc. Chem. Res.* **1988**, *21*, 407−413. (b) Lewis, N. S.; Wrighton, M. S. *Science* **1981**, *211*, 944−947.

(7) (a) Avila, A.; Gregory, B. W.; Niki, K.; Cotton, T. M. *J. Phys. Chem. B* **2000**, *104*, 2759−2766. (b) Feng, Z. Q.; Imabayashi, S.; Kakiuchi, T.; Niki, K. *J. Chem. Soc., Faraday Trans.* **1997**, *93*, 1367−1370. (c) Song, S.; Clark, R. A.; Bowden, E. F.; Tarlov, M. J. *J. Phys. Chem.* **1993**,*97*, 6564−6572. (d) Tarlov, M. J.; Bowden, E. F. *J. Am. Chem. Soc.* **1991**, *113*, 1847−1849.

(8) (a) Murgida, D. H.; Hildebrandt, P. *Angew. Chem., Int. Ed.* **2001**, *40*, 728−731.(b) Murgida, D. H.; Hildebrandt, P. *J. Mol. Struct.* **2001**, *565*, 97−100. (c) Murgida, D. H.; Hildebrandt, P. *J. Phys. Chem. B* **2001**, *105*, 1578−1586. (d) Murgida, D. H.; Hildebrandt, P. *J. Am. Chem. Soc.* **2001**, *123*, 4062−4068. (e) Murgida, D. H.; Hildebrandt, P. *J. Phys. Chem. B* **2002**, *106*, 12814−12819.

(9) (a) Liu, H. Y.; Yamamoto, H.; Wei, J. J.; Waldeck, D. H. *Langmuir* **2003**, *19*, 2378−2387. (b) Wei, J. J.; Liu, H. Y.; Khoshtariya, D. E.; Yamamoto, H.; Dick, A.; Waldeck, D. H. *Angew. Chem.,Int. Ed.* **2002**, *41*, 4700−4703. (c) Wei, J. J.; Liu, H. Y.; Dick, A. R.; Yamamoto, H.; He, Y. F.; Waldeck, D. H. *J. Am. Chem. Soc.* **2002**, *124*, 9591−9599. (d) Yamamoto, H.; Liu, H. Y.; Waldeck, D. H. *Chem. Commun.* **2001**, 1032−1033.

(10) Rivas, L.; Murgida, D. H.; Hildebrandt, P. *J. Phys. Chem. B* **2002**, *106*, 4823−4830.

(11) Wackerbarth, H.; Murgida, D. H.; Oellerich, S.; Döpner, S.; Rivas, L.; Hildebrandt, P. *J. Mol. Struct.* **2001**,*563*, 51−59.

(12) Oellerich, S.; Wackerbarth, H.; Hildebrandt, P. *J. Phys. Chem. B* **2002**, *106*, 6566−6580.

(13) Murgida, D. H.; Hildebrandt, P.; Smith, A. Unpublished results.

(14) Kneipp, K.; Kneipp, H.; Itzkan, I.; Dasari, R. R.; Feld, M. S. *J. Phy. Condens. Matter* **2002**, *14*, R597−R624.

(15) Brutigan, D. L.; Ferguson, S.; Margoliash, E. *Methods in Enzymology*; Fleischer, S., Packer, L., Eds.; Academic Press: New York, 1978; Vol. 53, pp 131−132.

(16) Wackerbarth, H.; Klar, U.; Günther, W.; Hildebrandt, P. *Appl. Spectrosc.* **1999**, *53*, 283−291.

(17) Clavilier, J.; Faure, R.; Guinet, G.; Durand, R. *J. Electroanal. Chem.* **1980**, *107*, 205−209.

(18) Sawyer, D. T.; Sobkowiak, A.; Roberts, J. L., Jr. *Experimental Electrochemistry for Chemists*; Wiley: New York, 1995; pp 74−75. The diffusion constant of $Fe(CN)_6^{3-/4-}$ is assumed to be 7.63×10^{-6} cm^2/sec.

(19) This calculation assumes a parallel plate model for the capacitance of the film ($C = \varepsilon\varepsilon_0/d$) and takes the alkanethiol dielectric constant ε to be 2.6.

(20) (a) Andreu, R.; Fawcett, W. R. *J. Phys. Chem.* **1994**, *98*, 12753−12758. (b) Porter, M. D.; Bright, T. B.; Allara, D. L.; Chidsey, C. E. D. *J. Am. Chem. Soc.* **1987**, *109*, 3559−3568.

(21) Döpner, S.; Hildebrandt, P.; Mauk, A. G.; Lenk, H.; Stempfle, W. *Spectrochim. Acta, Part AMol. Biomol. Spectrosc.* **1996**, *52*, 573−584.

(22) Terrettaz, S.; Cheng, J.; Miller, C. J. *J. Am. Chem. Soc.* **1996**, *118*, 7857−7858.

(23) The reduction was taken to be reversible. For a description of such an analysis see: Bard, A. J.; Faulkner, L. R. *Electrochemical Methods*; Wiley: New York, 1996.

(24) (a) Weiss, P. S.; Bumm, L. A.; Dunbar, T. D.; Burgin, T. P.; Tour, J. M.; Allara, D. L. *Ann. N.Y. Acad. Sci.***1998**, *852*, 145. (b)Gorman, C. B.; Carrol, R. L.; He, Y.; Tian, F.; Fuierer, R. *Langmuir* **2000**, *16*, 6312.

(25) Assigning these elevated structures to pyridine-terminated thiols yields a pyridine coverage of about 13 pmol/cm^2, assuming a coverage of 700 pmol/cm^2 for a compact alkanethiol monolayer on Au(111). A comparison of this pyridine coverage estimate to the electrochemically determined Cyt-*c* coverage indicates a pyridinyl/Cyt-*c* ratio of about 60. (a) Finklea, H. O. In *Electroanalytical Chemistry*; Bard, A. J., Ed.; Marcel Dekker: New York, 1996; pp 109−335; (b) Walczak, M. M.; Popenoe, D. D.; Deinhammer, R. S.; Lamp, B. D.; Chung, C. K.; Porter, M. D. *Langmuir* **1991**, *7*, 2687−2693.

(26) Fan, C. H.; Gillespie, B.; Wang, G. M.; Heeger, A. J.; Plaxco, K. W. *J. Phys. Chem. B* **2002**, *106*, 11375−11383.

(27) Döpner, S.; Hildebrandt, P.; Rosell, F. I.; Mauk, A. G. *J. Am. Chem. Soc.* **1998**, *120*, 11246−11255.

(28) (a) Laibinis, P. E.; Whitesides, G. M.; Allara, D. L.; Tao, Y. T.; Parikh, A. N.; Nuzzo, R. G. *J. Am. Chem. Soc.***1991**, *113*, 7152−7167. (b) Walczak, M. M.; Chung, C. K.; Stole, S. M.; Widrig, C. A.; Porter, M. D. *J. Am. Chem. Soc.* **1991**, *113*, 2370−2378.

(29) Murgida, D. H.; di Paolo, R.; Hildebrandt, P. Unpublished results.

(30) (a) Cytochrome *c*: PDB 1AKK. Primary citation: Banci, L.; Bertini, I.; Gray, H. B.; Luchinat, C.; Reddig, T.; Rosato, A.; Turano, P. *Biochemistry* **1997,** *36*, 9867. (b) Complex with imidazole: PDB 1FI7. Primary citation: Banci, L.; Bertini, I.; Liu, G. H.; Reddig, T.; Tang, W. X.; Wu, Y. B.; Yao, Y.; Zhu, D. X.*J. Biol. Inorg. Chem*. **2001**, *6*, 628.